JACS
JOURNAL OF THE AMERICAN CHEMICAL SOCIETY
Article
pubs.acs.org/JACS

Adsorption Mechanism of Inhibitor and Guest Molecules on the Surface of Gas Hydrates

Takuma Yagasaki,[†] Masakazu Matsumoto,[†] and Hideki Tanaka*[,†,‡]

[†]Department of Chemistry, Faculty of Science, Okayama University, Okayama, 700-8530, Japan
[‡]Research Center of New Functional Materials for Energy Production, Storage and Transport, Okayama, 700-8530, Japan

Supporting Information

ABSTRACT: The adsorption of guest and kinetic inhibitor molecules on the surface of methane hydrate is investigated by using molecular dynamics simulations. We calculate the free energy profile for transferring a solute molecule from bulk water to the hydrate surface for various molecules. Spherical solutes with a diameter of ∼0.5 nm are significantly stabilized at the hydrate surface, whereas smaller and larger solutes exhibit lower adsorption affinity than the solutes of intermediate size. The range of the attractive force is subnanoscale, implying that this force has no effect on the macroscopic mass transfer of guest molecules in crystal growth processes of gas hydrates. We also examine the adsorption mechanism of a kinetic hydrate inhibitor. It is found that a monomer of the kinetic hydrate inhibitor is strongly adsorbed on the hydrate surface. However, the hydrogen bonding between the amide group of the inhibitor and water molecules on the hydrate surface, which was believed to be the driving force for the adsorption, makes no contribution to the adsorption affinity. The preferential adsorption of both the kinetic inhibitor and the spherical molecules to the surface is mainly due to the entropic stabilization arising from the presence of cavities at the hydrate surface. The dependence of surface affinity on the size of adsorbed molecules is also explained by this mechanism.

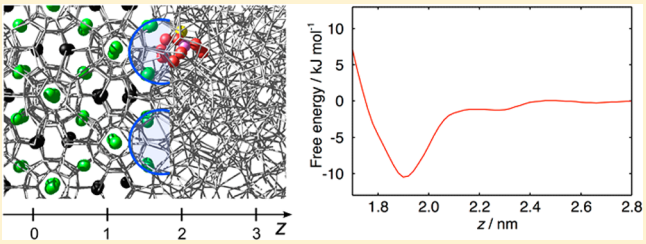

INTRODUCTION

Gas hydrates are crystalline solids consisting of water and guest molecules such as methane.[1,2] In gas hydrates, water molecules form a three-dimensional crystal lattice with cages which accommodate guest molecules. Most gas hydrates are classified into either structure I or II. Structure I hydrate contains 5^{12} and $5^{12}6^2$ cages and structure II hydrate consists of 5^{12} and $5^{12}6^4$ cages. Gas hydrates are stable under high-pressure and low-temperature conditions. There are a huge amount of natural gas hydrates in ocean sediments, and they are expected to be a future energy resource.[2−4] It has also been proposed that gas hydrates can be used for gas separation, storage, and transportation.[2,5−10]

Understanding of microscopic mechanism of crystal growth is essential for the effective utilization of gas hydrates, and there have been a number of molecular dynamics (MD) studies.[11−41] Due to its hydrophobicity, the concentration of guest species in the aqueous phase is quite low even under high pressures. It is expected that attachment of each guest molecule on the hydrate surface occurs independently. Crystal growth of gas hydrates thus can be interpreted as successive intermittent adsorption of a guest molecule on the hydrate surface. However, early simulation studies have focused only on the hydrate growth in supersaturated solutions of guest species, and therefore details of each adsorption process, such as the strength and range of the adsorption force, remain unresolved.

The adsorption of a molecule on the hydrate surface is also important in terms of inhibition of hydrate formation. Plugging of oil and gas pipelines is a serious industrial problem caused by hydrate formation.[1,2] A traditional way to avoid the plugging is the addition of thermodynamic inhibitors (TI) such as methanol or NaCl. TIs lower the hydrate/liquid/gas three phase equilibrium temperature.[1] In addition, TIs increase the dissociation rate of gas hydrates because they facilitate formation of bubbles which can reduce the supersaturation of guest molecules in the aqueous phase near the hydrate.[42,43] An alternative way is the use of low dosage hydrate inhibitors (LDHI).[44,45] LDHIs do not lower the three phase equilibrium temperature but kinetically inhibit the formation of hydrate plugs. Usually, LDHIs are dosed at a concentration of only 0.1−1.0 wt %, whereas TIs are dosed at 20−50 wt %, and thus LDHIs are economically more favorable.[44] It has been suggested that LDHIs bind to the hydrate surface, and the efficiency of them depends on the adsorption affinity.[44−48] MD simulations have been employed to examine the inhibition mechanism of LDHIs.[48−59]

Kinetic hydrate inhibitors (KHI) belong to a type of LDHI. KHIs are water-soluble polymers that inhibit formation and growth of hydrate crystal. Efficient KHIs are reported to commonly have both amide groups and hydrophobic parts. A conventional picture on the origin of their effect is that the adsorption of KHIs is mainly due to the hydrogen bonds between the amide groups and water molecules on the hydrate

Received: July 16, 2015
Published: September 2, 2015

DOI: 10.1021/jacs.5b07417
J. Am. Chem. Soc. 2015, 137, 12079−12085

surface.[44,45] Carver et al. demonstrated that the adsorption of monomers of KHIs occurs through the hydrogen bonds between the amide group and the hydrate surface in their simulation studies.[50,51] However, their simulations were performed only for the hydrate/vapor interface. KHIs are water-soluble and bind to the hydrate/water interface. It is not sure as to whether the adsorption on the hydrate/vapor interface is similar to that on the hydrate/water interface.

In this paper, we investigate the adsorption of various molecules on the hydrate surface using MD simulations. We calculate the free energy and energy profiles for a solute molecule dissolved in liquid water against distance from the surface of methane hydrate. The simulation is performed for a methane molecule, a monomer of a KHI, and several fictitious molecules. We demonstrate that the adsorption affinity strongly depends on the size of solute molecule and that the range of the attraction is subnanoscale. It is found that the conventional picture for the adsorption of KHIs is incorrect, that is, the amide hydrogen bonding does not contribute to the adsorption affinity. The driving force of the adsorption and the dependence on molecular size are discussed in terms of the hydration entropy. We show it is the surface structure that gives rise to the preferential adsorption of molecules having the diameter similar to the cage size in the hydrate.

COMPUTATIONAL DETAILS

MD simulations are performed using the GROMACS 4.6 package, and the particle mesh Ewald method is used to treat long-range coulomb interactions.[60,61] The system consists of a slab of hydrate and an aqueous solution in which a solute molecule is dissolved. The hydrate slab is a 2 × 2 × 2 unit cell replica of fully occupied structure II methane hydrate (1088 water molecules and 192 methane molecules). Although pure methane forms structure I hydrate, we choose structure II in this study because natural gases, i.e., mixtures of methane and a small amount of larger molecules such as propane, often form structure II hydrate and a number of experimental studies on KHIs have been performed for this type of hydrates.[1,44] The number of water molecules in the liquid phase is 2162. The size of the simulation cell is roughly 3.4 × 3.4 × 9.6 nm^3. A snapshot of the simulation cell is shown in Figure 1. The z coordinate of the center of mass of all guest molecules in the hydrate is defined as $z = 0$.

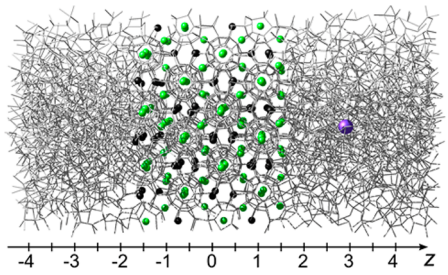

Figure 1. Snapshot of the simulation cell. A hydrogen-bond network of water is represented by lines. Green and black spheres are the guest molecules in small (5^{12}) and large ($5^{12}6^4$) cages of the hydrate slab. A solute molecule located at $z = 2.9$ nm is shown as a purple sphere.

We employ the TIP4P/2005 model for water and the OPLS united-atom model for methane.[62,63] The temperature and the pressure are kept at 275 K and 400 bar, which is a hydrate/liquid/gas three phase equilibrium condition of structure I methane hydrate for the combination of the TIP4P/2005 and OPLS models.[20] Note that the thermodynamic stability of structure II methane hydrate is almost equivalent to that of structure I methane hydrate.[1,64,65] To prevent the hydrate from local melting, all methane molecules in the hydrate slab are fixed at the lattice points using a harmonic potential with a force constant of 10,000 kJ mol^{-1} nm^{-2}.

We calculate the free energy profiles of a solute molecule approaching a (001) facet of structure II methane hydrate from the umbrella sampling technique with the weighted histogram analysis method.[66,67] The solute molecule is bound around a given z value using a harmonic potential with a force constant of 1000 kJ mol^{-1} nm^{-2}. No constraints are applied to the x and y directions. The simulation is carried out for every 0.02 nm in the z direction. Each simulation is performed for at least 20 ns.

The free energy profiles are calculated for spherical solutes with various sizes. The spherical solutes are variants of methane; the diameter of the spherical molecule, σ, is varied, whereas the depth of the LJ potential, ϵ, is fixed at the value for methane, 1.23 kJ mol^{-1}.[63] We also calculate the free energy profile of a monomer of polyvinylcaprolactam (PVCap). PVCap is an efficient KHI and has been used as a standard substance for comparison with newly developed KHIs.[44,45] Because the C−C bonds in the main chain of PVCap are single bonds, we assume *N*-ethylcaprolactam instead of vinylcaprolactam as a monomer of PVCap. A similar assumption was made in an early MD study on a different KHI, polyvinylpyrrolidone (PVP).[50] The parameters for the intramolecular and Lennard-Jones (LJ) potentials of the PVCap monomer are taken from the AMBER force field and the OPLS united-atom model, respectively.[68,69] To determine the partial charges on each atom, we evaluate the electrostatic potential derived charges at the B3LYP/6-31G(d,p) level of theory with the polarizable continuum model using the Gaussian 09 package.[70] The electrostatic potential derived charges are evaluated from the Merz−Singh−Kollman scheme.[71,72] The obtained charges are shown in Figure 2. The amide oxygen can form hydrogen

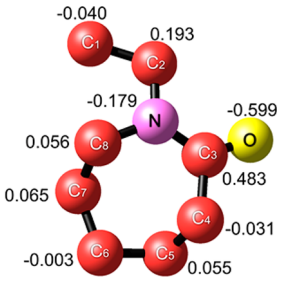

Figure 2. Partial charges on the monomer of PVCap.

bonds with surrounding water molecules because of the large negative charge. In order to examine the effect of the amide hydrogen bonding, we also calculate the free energy profile of a fictitious nonpolar PVCap monomer. Intramolecular and LJ potential parameters for the nonpolar PVcap monomer are the same as those for the normal PVCap monomer but all partial charges on the nonpolar monomer are set to zero.

RESULTS AND DISCUSSION

Figure 3a shows the free energy profile, $\Delta G(z) = G(z) - G(\infty)$, for transferring a solute methane molecule from bulk liquid water to the hydrate surface. A deep minimum is found at $z = 1.68$ nm. Figure 3b displays a snapshot of the solute molecule bound at $z = 1.68$ nm. The outermost layer of the hydrate slab consists of filled small cages, and there are open large cages on the hydrate surface. The solute molecule at $z = 1.68$ nm is in such an open large cage and continues to stay there during the simulation time of 20 ns. The free energy $\Delta G(z)$ is negative for 1.56 nm < z < 2.25 nm. The width of this region, 0.69 nm, is negligible compared to the macroscopic length scale. As shown below, a similar result is obtained for other molecules. That is, in a crystal growth process, there is no long-range force attracting dissolved guest molecules to the

DOI: 10.1021/jacs.5b07417
J. Am. Chem. Soc. 2015, 137, 12079−12085

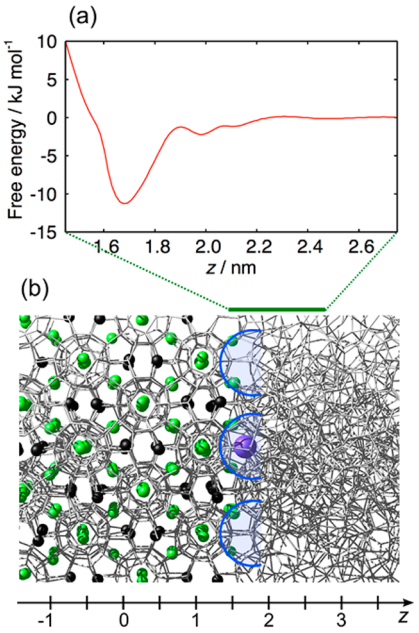

Figure 3. (a) Free energy profile for transferring a solute methane molecule from bulk water to the hydrate surface. (b) Snapshot of the solute methane molecule bound at z = 1.68 nm. The solute molecule is shown as large purple sphere. Green and black spheres are the guest molecules in small and large cages of the hydrate slab. Blue arcs indicate the open large cages on the hydrate surface.

hydrate surface (note that there might be macroscopic effects such as concentration gradient in real systems).

In order to examine the dependence of the adsorption affinity on the size of the solute molecule, we calculate the free energy profiles of spherical LJ molecules of various sizes. The results for three diameters are shown in Figure 4a–c. The solute molecule with a diameter of 0.273 nm is smaller than

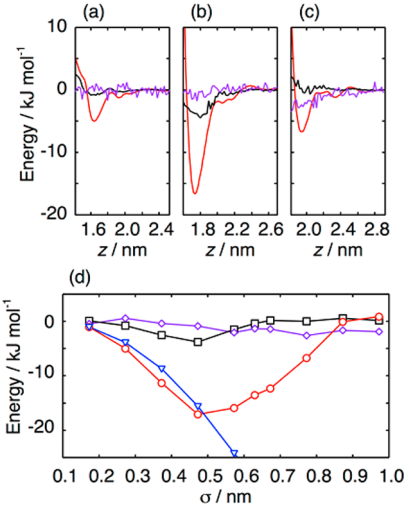

Figure 4. Energy profiles for the solute molecule with σ = (a) 0.273, (b) 0.473, and (c) 0.773 nm. Changes in the free energy ΔG, solute energy ΔE_u, and volume $P\Delta V$ are plotted with red, black, and purple curves, respectively. (d) The σ dependence of the thermodynamic quantities at the minimum of the free energy profile, $z = z_m$. Red circles, black squares, and purple diamonds are $\Delta G(z_m)$, $\Delta E_u(z_m)$, and $P\Delta V(z_m)$, respectively. Blue triangles show the dehydration free energies.

methane by 0.1 nm. Although this molecule is also stabilized at the surface of methane hydrate, the adsorption affinity of this molecule, 5 kJ mol^{-1} (Figure 4a), is smaller than that of methane, 12 kJ mol^{-1} (Figure 3a). In contrast, the solute molecule with a diameter of 0.473 nm exhibits a higher adsorption affinity than methane (Figure 4b). An even larger molecule, σ = 0.773 nm, in turn shows a small affinity of 6 kJ mol^{-1} (Figure 4c). Figure 4d summarizes the difference between the free energies of the solute molecule at the minimum ($z = z_m$) and that in bulk water, $\Delta G(z_m) = G(z_m) - G(\infty)$, for all spherical solutes examined in this study. As the diameter σ increases, the adsorption affinity, $-\Delta G(z_m)$, increases for σ < 0.473 nm, and then it turns to decrease.

Figure 4a–c also shows the energy profile of the solute, $\Delta E_u(z) = E_u(z) - E_u(\infty)$, where E_u is the interaction energy between the solute and all other molecules, and the volume profile, $P\Delta V(z) = PV(z) - PV(\infty)$, where $V(z)$ is the average volume of the entire system calculated from the NPT simulation in which the solute is fixed at z and P is the pressure specified in the NPT simulation, i.e., 400 bar. Although these terms contribute to the adsorption affinity of the spherical LJ solutes, they are much smaller than the free energy change $\Delta G(z_m)$. For example, the sum of $\Delta E_u(z_m)$ and $P\Delta V(z_m)$ is only 1/4 of $\Delta G(z_m)$ for the solute with σ = 0.473 nm.

The size dependence of the adsorption affinity can be explained in terms of the hydration of hard sphere solutes. The hydration free energy of a hard sphere with a diameter d is given by

$$G_d^H = -kT \ln P_d \tag{1}$$

where P_d is the insertion probability which is defined as the ratio of the volume of cavities that can accommodate the hard sphere solute in a unit volume.[73,74] Because a hard sphere has no attractive interaction with solvent molecules, G_d^H is purely entropic (see Supporting Information for more details).[74−77] Eq 1 expresses the free energy for hydration in a uniform liquid. When the hydration free energy depends on the z coordinate, the free energy profile of the hard sphere can be expressed as

$$\Delta G_d^H(z) = G_d^H(z) - G_d^H(\infty) = -kT \ln \frac{P_d(z)}{P_d(\infty)} \tag{2}$$

where $P_d(z)$ is the z dependent insertion probability. This equation indicates that the solute molecule can be entropically stabilized at the hydrate surface without any direct attractive interactions between the solute and the surface when the insertion probability is higher at the surface than in bulk water. Figure 3b shows that this is indeed the case; as indicated by blue arcs, there are empty open cages on the hydrate surface each of which can accommodate a solute molecule.

Figure 5 illustrates the size dependence of the adsorption affinity of spherical molecules. For simplicity, the hard sphere diameters of water and solute are approximated to 0.158 nm[62] and σ of each solute, respectively. The size of solute A in Figure 5 is comparable to the voids in the hydrogen-bond network of liquid water, and thus the insertion probability in bulk water, $P_d(\infty)$, is high. The insertion probability at the hydrate surface, $P_d(z_m)$, is also high because this solute is smaller than the cavities at the hydrate surface. Since $P_d(z_m)$ is close to $P_d(\infty)$, the adsorption free energy of solute A is quite small (the leftmost point in Figure 4d). Solute B is a model of the spherical solute with σ = 0.473 nm. Because this solute is larger

DOI: 10.1021/jacs.5b07417
J. Am. Chem. Soc. 2015, 137, 12079−12085

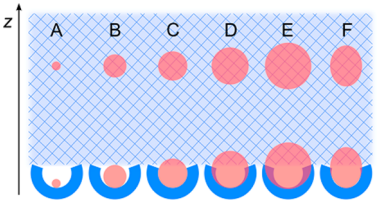

Figure 5. Schematic of stabilization mechanism of solutes on the hydrate surface due to the presence of cavities. Blue arcs are the open large cages on the hydrate surface. The inner diameter of the large cage is 0.63 nm. This value is obtained from a standard value for the diameter (O−O distance) of the large cage in structure II hydrate, 0.946 nm,[1] and the van der Waals radius of the employed water model, 0.158 nm.[62] Solutes A−E represent the spherical LJ solutes with σ = 0.173, 0.473, 0.630, 0.773, and 0.973 nm. A nonspherical solute F is a model of the monomer of PVCap. The blue net represents the hydrogen-bond network in liquid water.

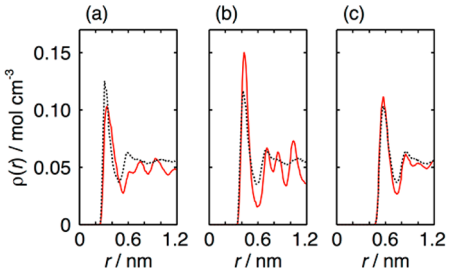

Figure 6. Radial density functions of water around the spherical LJ solute at the hydrate surface (red) and in bulk water (black). Panels a−c are the results for the solute with σ = 0.273, 0.473, and 0.773 nm, respectively.

than the size of a typical void that occurs in liquid water, $P_d(\infty)$ is much lower than 1. In contrast, $P_d(z_m)$ is still high because this solute can be completely included in an open cage at the surface. As a result, the solute molecule with σ = 0.473 nm is remarkably stabilized at the hydrate surface. Size of solute C perfectly matches the inner diameter of the large cage, 0.63 nm. The adsorption affinity of this solute (σ = 0.63 nm) is smaller than that of solute B (σ = 0.473 nm) because the upper part of solute C is exposed to liquid water. The diameter of solute D, σ = 0.773 nm, is somewhat larger than the inner diameter of the large cage. Because the cages at the hydrate surface are open and flexible, this molecule is still weakly stabilized at the surface (Figure 4c). The flexibility of the cages is, of course, limited. For very large molecule like solute E, the presence of the cage structure results in a very low $P_d(z_m)$. $P_d(\infty)$ is also quite low but higher than $P_d(z_m)$ because there is no stable and persisting structure like hydrate cages that prevents formation of large cavities in liquid water. Therefore, very large spherical solutes are not adsorbed on the hydrate surface (the rightmost point in Figure 4d).

If this mechanism is correct, the free energy for the transfer of a solute from bulk water to the hydrate surface, $\Delta G(z_m)$, would be almost identical to that for the transfer of the solute from bulk water to the vapor phase, i.e., the dehydration free energy G_{deh}, for small molecules like solute A and B in Figure 5. We perform MD simulations with a system consisting of a solute molecule and 1000 water molecules and calculate G_{deh} of the spherical LJ solutes using the acceptance ratio method with the soft core form of potentials.[78,79] The dehydration free energies, G_{deh}, are shown as blue triangles in Figure 4d. We see that G_{deh} is indeed similar to $\Delta G(z_m)$ for σ < ~0.5 nm. $\Delta G(z_m)$ is slightly lower than G_{deh} because the solute in the open cage is stabilized by the van der Waals interactions with surrounding water molecules, whereas there are no solute−solvent interactions in the vapor phase.

A solute is fully or partially contained in an open cages at $z = z_m$, and thus the volume of the system decreases as the solute approaches the surface. Needless to say, this effect is larger for larger solutes as shown in Figure 4d. Figure 4d also shows that the energetic stabilization at the surface, $\Delta E_u(z_m)$, is largest for the solute of intermediate size, σ = 0.473 nm. The radial density functions of water around the spherical solutes, $\rho(r)$, are presented in Figure 6. We see that peaks in $\rho(r)$ for the solute with σ = 0.473 nm are pronounced at the surface (Figure 6b). Due to the sharp first peak, the van der Waals interaction between the solute and water molecules is stronger at the surface than in bulk water. The pronounced first peak is not observed for the solute with σ = 0.773 nm because this solute is larger than the cage (Figure 6c). The first peak of the solute with σ = 0.273 nm is lower and broader at the surface because this molecule is small and moves around in the cage (Figure 6a). Therefore, the energetic stabilization is significant only for molecules of medium size.

Next, we discuss the adsorption mechanism of a more complicated molecule, PVCap. The free energy profile of the PVCap monomer is shown as a solid red curve in Figure 7. A

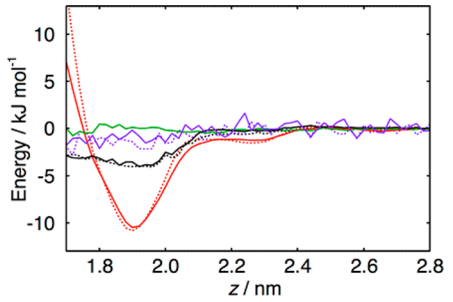

Figure 7. Energy profiles of the PVCap monomer (solid) and the fictitious nonpolar PVCap monomer (dotted). Red and purple curves are the changes in the free energy and PV for the transfer of the PVCap monomer. The change in the interaction energy between the solute and surrounding molecules is divided into the LJ part (black) and the coulomb part (green).

deep minimum is found at z = 1.90 nm (this value is larger than the minimum position for methane, z = 1.68 nm, simply because the location of a solute is defined by the center of mass and the PVCap monomer is larger than methane). This monomer is stabilized at the hydrate surface by 10.5 kJ mol^{-1}. A typical snapshot of the monomer at z = 1.90 nm is shown in Figure 8a. The monomer of PVCap prefers an open large cage on the hydrate surface. It is found that the monomer at z = 1.90 nm keeps inside the large cage during the simulation time of 70 ns, although no constrains are imposed along the x and y directions.

A monomer of PVCap has an amide group. It has been believed that the surface affinity of KHIs arises from the hydrogen bonds between the amide oxygen and water molecules on the hydrate surface.[44,45,48,50,51] To evaluate the significance of the amide hydrogen bonding, we calculate the free energy profile of the fictitious nonpolar PVCap monomer. The nonpolar PVCap monomer cannot form hydrogen bonds with water because all partial charges on the monomer are set

DOI: 10.1021/jacs.5b07417
J. Am. Chem. Soc. 2015, 137, 12079−12085

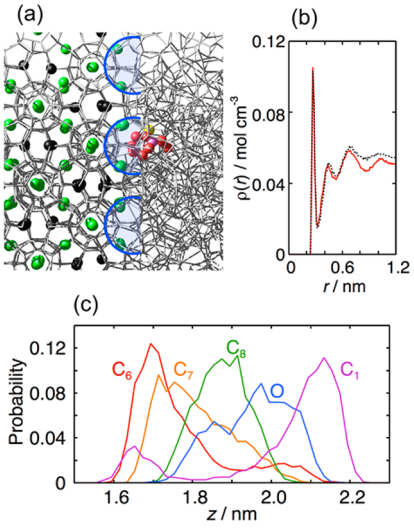

Figure 8. (a) Snapshot of the PVCap monomer at z = 1.90 nm. Blue arcs indicate the open large cages on the hydrate surface. (b) Radial density functions of water molecules around the amide oxygen of the PVCap monomer at the hydrate surface (red) and in bulk water (black). (c) Distribution functions of several atoms in the PVCap monomer at z = 1.90 nm.

to zero. Figure 7 demonstrates that the free energy profile of the nonpolar monomer is quite similar to that of the original monomer. This result indicates that the amide hydrogen bonding is insignificant for the adsorption of KHIs on the hydrate surface. Figure 7 also presents the energy profiles of the PVCap monomers. The coulomb part of the energy does not change in transferring the PVCap monomer from bulk water to the hydrate surface. The amide group can form hydrogen bonds with water molecules on the hydrate surface, but it can also form hydrogen bonds with liquid water. There is no rationale for a stronger hydrogen bonding in the former than in the latter. As shown in Figure 8b, the first peak of the radial density function of water molecules around the amide oxygen of the PVCap monomer at the hydrate surface is almost identical to that in bulk water. Therefore, the amide hydrogen bonding makes no contribution to the adsorption affinity. It should be noted that the amide groups in KHIs are unnecessary for the adsorption but essential for the solubility. Nonpolar molecules do not act as KHIs because they are insoluble in water and cannot reach the hydrate/water interface.

Figure 7 shows that the change in PV term by the transfer of the monomer is very small. The LJ part of the energy is stabilized at the surface by 3.5 kJ mol^{-1}. This is only 33% of the free energy change. The surface preference of the PVCap monomer is also mainly due to the entropic stabilization caused by the presence of cavities at the hydrate surface. The distance between C_1 and C_6 (Figure 2) is roughly 0.49 nm. Because the van der Waal radii of these carbons are 0.1955 and 0.19525 nm,[69] the height of the monomer is ∼0.88 nm. This value is much larger than the inner diameter of the large cage, 0.63 nm. However, the width of the monomer is comparable to the inner diameter. The distance between C_4 and C_7 is ∼0.3 nm, and this yields a width of ∼0.69 nm. Thus, the PVCap monomer is partially incorporated in an open cage and stabilized at the hydrate surface as illustrated in Figure 5. Figure 8c shows the distribution of several atoms in the PVCap monomer bound at z = 1.9 nm. The distribution function of C_6 has a large peak at z = 1.7 nm. This indicates that this atom is inside a large cage on the surface in most cases. C_7 is also located in the large cage. The distribution functions of C_5 and C_4 are similar to those of C_6 and C_7, respectively (not shown). The distribution functions of C_1 and C_2 (not shown) show a small peak at z = 1.7 nm together with a large peak at z = 2.1 nm, indicating that C_1−C_2 is located in the open large cage instead of C_4−C_7 in some cases. Experimental studies reported that the addition of a methyl group to the main chain increases the performance of some KHIs.[44] The present result may support this experimental observation, although the simulation is performed for a monomer. The oxygen atom of the PVCap monomer dislikes being inside the cage on the hydrate surface. This is consistent with the fact that enclosing a hydrophilic molecule, such as methanol, in a hydrate cage results in a large destabilization of the hydrate.[80−84]

CONCLUSIONS

We have investigated the adsorption of molecules on the interface between methane hydrate and liquid water using MD simulations. The free energy profile for transferring a solute molecule from bulk water to the hydrate surface is calculated for various molecules. The surface affinities of medium size molecules are quite large, whereas smaller and larger molecules are weakly or not adsorbed on the surface. The range of the attractive force is subnanoscale, and thus this force has no effect on the macroscopic mass transfer of guest molecules in crystal growth processes of gas hydrates. The monomer of PVCap is also stabilized at the hydrate surface. The amide hydrogen bonding makes no contribution to the adsorption affinity, although it was believed to be the driving force for the adsorption of KHIs. For both the spherical solutes and the KHI monomer, the surface preference is largely due to the entropic stabilization arising from the presence of cavities at the hydrate surface. The present results may shed new light on the development of novel efficient KHIs.

In this study, we have focused on the adsorption of molecules on a (001) facet of structure II hydrate. The composition and arrangement of open cages at the surface depend on crystallographic plane and type of hydrate structures. Adsorption affinities for different surfaces would be different from that for the (001) facet. This effect might be more significant for KHI polymers than for the corresponding monomers because the matching between the interval of side chains and the pattern of cages on the hydrate surface would be important for the adsorption affinity. The adsorption affinities of each hydrophobic group of a KHI polymer may be independent from each other. However, it is likely to occur that the adsorption of a hydrophobic group of the polymer in a cage at the hydrate surface enhances the structure around the cage, and it results in a strong adsorption in the neighbor cages compared with the adsorption of an isolated monomer. If so, a polymer (or oligomer) designed to maximize this concerted effect would exhibit outstanding performance as an inhibitor of hydrate growth. Further simulations are required for comprehensive understanding of adsorption mechanism of polymeric KHIs.

There are two types of LDHIs: KHIs and antiagglomerants (AAs).[44,45] AAs also adsorb on the hydrate surface and prevent hydrate particles from agglomerating. The adsorption mechanism shown in this study is presumably relevant to the mechanism of AAs because they also have hydrophobic groups that can be partially included in open cages at the hydrate surface. The findings in this study might also provide some

DOI: 10.1021/jacs.5b07417
J. Am. Chem. Soc. 2015, 137, 12079−12085

insights into the formation process of semiclathrate hydrates which have received much attention in recent years because of their possible applications in gas storage, gas separation, and cold storage.[85−87] Free energy calculations would yield a wealth of information on these systems.

■ ASSOCIATED CONTENT

Supporting Information

The Supporting Information is available free of charge on the ACS Publications website at DOI: 10.1021/jacs.5b07417.

Optimized structure and the energy of the monomer of PVCap obtained from the electronic structure calculation and the decomposition of the free energy (PDF)

■ AUTHOR INFORMATION

Corresponding Author

*htanakaa@okayama-u.ac.jp

Notes

The authors declare no competing financial interest.

■ ACKNOWLEDGMENTS

The present work was supported by a Grant-in-Aid by JSPS and by HPCI Strategic Programs for Innovative Research (SPIRE) and Computational Materials Science Initiative (CMSI), MEXT, Japan. Calculations were performed at Research Center for Computational Science, Okazaki, Japan, and the K computer at the RIKEN Advanced Institute for Computational Science (Project ID: hp140216).

■ REFERENCES

(1) Sloan, E. D.; Koh, C. A. *Clathrate Hydrates of Natural Gases*; CPC Press: Boca Raton, 2008.
(2) Sloan, E. D. *Nature* **2003**, *426*, 353.
(3) Kvenvolden, K. A. *Ann. N. Y. Acad. Sci.* **2000**, *912*, 17.
(4) Boswell, R. *J. Pet. Sci. Eng.* **2007**, *56*, 9.
(5) Mao, W. L.; Mao, H.-k.; Goncharov, A. F.; Struzhkin, V. V.; Guo, Q.; Hu, J.; Shu, J.; Hemley, R. J.; Somayazulu, M.; Zhao, Y. *Science* **2002**, *297*, 2247.
(6) Mao, W. L.; Mao, H. K. *Proc. Natl. Acad. Sci. U. S. A.* **2004**, *101*, 708.
(7) Struzhkin, V. V.; Militzer, B.; Mao, W. L.; Mao, H. K.; Hemley, R. J. *Chem. Rev.* **2007**, *107*, 4133.
(8) Florusse, L. J.; Peters, C. J.; Schoonman, J.; Hester, K. C.; Koh, C. A.; Dec, S. F.; Marsh, K. N.; Sloan, E. D. *Science* **2004**, *306*, 469.
(9) Kang, S.-P.; Lee, H. *Environ. Sci. Technol.* **2000**, *34*, 4397.
(10) Linga, P.; Kumar, R.; Englezos, P. *J. Hazard. Mater.* **2007**, *149*, 625.
(11) Tse, J. S.; Klein, M. L.; McDonald, I. R. *J. Chem. Phys.* **1984**, *81*, 6146.
(12) Tse, J. S.; Klug, D. D. *J. Supramol. Chem.* **2002**, *2*, 467.
(13) English, N. J.; MacElroy, J. M. D. *J. Chem. Phys.* **2004**, *120*, 10247.
(14) Vatamanu, J.; Kusalik, P. G. *J. Phys. Chem. B* **2006**, *110*, 15896.
(15) Vatamanu, J.; Kusalik, P. G. *J. Phys. Chem. B* **2008**, *112*, 2399.
(16) Nada, H. *J. Phys. Chem. B* **2006**, *110*, 16526.
(17) Nada, H. *J. Phys. Chem. B* **2009**, *113*, 4790.
(18) Tung, Y. T.; Chen, L. J.; Chen, Y. P.; Lin, S. T. *J. Phys. Chem. B* **2010**, *114*, 10804.
(19) Tung, Y.-T.; Chen, L.-J.; Chen, Y.-P.; Lin, S.-T. *J. Phys. Chem. B* **2012**, *116*, 14115.
(20) Conde, M. M.; Vega, C. *J. Chem. Phys.* **2010**, *133*, 064507.
(21) Michalis, V. K.; Costandy, J.; Tsimpanogiannis, I. N.; Stubos, A. K.; Economou, I. G. *J. Chem. Phys.* **2015**, *142*, 044501.
(22) Wu, J.-Y.; Chen, L.-J.; Chen, Y.-P.; Lin, S.-T. *J. Phys. Chem. C* **2015**, *119*, 1400.
(23) Moon, C.; Taylor, P. C.; Rodger, P. M. *J. Am. Chem. Soc.* **2003**, *125*, 4706.
(24) Hawtin, R. W.; Quigley, D.; Rodger, P. M. *Phys. Chem. Chem. Phys.* **2008**, *10*, 4853.
(25) Vatamanu, J.; Kusalik, P. G. *J. Am. Chem. Soc.* **2006**, *128*, 15588.
(26) Liang, S.; Rozmanov, D.; Kusalik, P. G. *Phys. Chem. Chem. Phys.* **2011**, *13*, 19856.
(27) Liang, S.; Kusalik, P. G. *J. Phys. Chem. B* **2013**, *117*, 1403.
(28) Pirzadeh, P.; Kusalik, P. G. *J. Am. Chem. Soc.* **2013**, *135*, 7278.
(29) Walsh, M. R.; Beckham, G. T.; Koh, C. A.; Sloan, E. D.; Wu, D. T.; Sum, A. K. *J. Phys. Chem. C* **2011**, *115*, 21241.
(30) Walsh, M. R.; Koh, C. A.; Sloan, E. D.; Sum, A. K.; Wu, D. T. *Science* **2009**, *326*, 1095.
(31) Zhang, Z.; Walsh, M. R.; Guo, G. J. *Phys. Chem. Chem. Phys.* **2015**, *17*, 8870.
(32) Jacobson, L. C.; Hujo, W.; Molinero, V. *J. Am. Chem. Soc.* **2010**, *132*, 11806.
(33) Jacobson, L. C.; Molinero, V. *J. Am. Chem. Soc.* **2011**, *133*, 6458.
(34) Knott, B. C.; Molinero, V.; Doherty, M. F.; Peters, B. *J. Am. Chem. Soc.* **2012**, *134*, 19544.
(35) Sarupria, S.; Debenedetti, P. G. *J. Phys. Chem. Lett.* **2012**, *3*, 2942.
(36) Jiménez-Ángeles, F.; Firoozabadi, A. *J. Phys. Chem. C* **2014**, *118*, 11310.
(37) Jiménez-Ángeles, F.; Firoozabadi, A. *J. Phys. Chem. C* **2015**, *119*, 8798.
(38) Lauricella, M.; Meloni, S.; English, N. J.; Peters, B.; Ciccotti, G. *J. Phys. Chem. C* **2014**, *118*, 22847.
(39) English, N. J.; Lauricella, M.; Meloni, S. *J. Chem. Phys.* **2014**, *140*, 204714.
(40) Zhao, W.-H.; Wang, L.; Bai, J.; Yuan, L.-F.; Yang, J.; Zeng, X. C. *Acc. Chem. Res.* **2014**, *47*, 2505.
(41) Bai, J.; Angell, C. A.; Zeng, X. C. *Proc. Natl. Acad. Sci. U. S. A.* **2010**, *107*, 5718.
(42) Yagasaki, T.; Matsumoto, M.; Andoh, Y.; Okazaki, S.; Tanaka, H. *J. Phys. Chem. B* **2014**, *118*, 11797.
(43) Yagasaki, T.; Matsumoto, M.; Andoh, Y.; Okazaki, S.; Tanaka, H. *J. Phys. Chem. B* **2014**, *118*, 1900.
(44) Kelland, M. A. *Energy Fuels* **2006**, *20*, 825.
(45) Perrin, A.; Musa, O. M.; Steed, J. W. *Chem. Soc. Rev.* **2013**, *42*, 1996.
(46) King, H. E.; Hutter, J. L.; Lin, M. Y.; Sun, T. *J. Chem. Phys.* **2000**, *112*, 2523.
(47) Larsen, R.; Knight, C. A.; Sloan, E. D., Jr *Fluid Phase Equilib.* **1998**, *150−151*, 353.
(48) Anderson, B. J.; Tester, J. W.; Borghi, G. P.; Trout, B. L. *J. Am. Chem. Soc.* **2005**, *127*, 17852.
(49) Carver, T. J.; Drew, M. G. B.; Rodger, P. M. *Ann. N. Y. Acad. Sci.* **2000**, *912*, 658.
(50) Carver, T. J.; Drew, M. G. B.; Rodger, P. M. *J. Chem. Soc., Faraday Trans.* **1996**, *92*, 5029.
(51) Carver, T. J.; Drew, M. G. B.; Rodger, P. M. *J. Chem. Soc., Faraday Trans.* **1995**, *91*, 3449.
(52) Freer, E. M.; Sloan, E. D. *Ann. N. Y. Acad. Sci.* **2000**, *912*, 651.
(53) Storr, M. T.; Taylor, P. C.; Monfort, J.-P.; Rodger, P. M. *J. Am. Chem. Soc.* **2004**, *126*, 1569.
(54) Storr, M. T.; Rodger, P. M. *Ann. N. Y. Acad. Sci.* **2000**, *912*, 669.
(55) Kvamme, B.; Kuznetsova, T.; Aasoldsen, K. *J. Mol. Graphics Modell.* **2005**, *23*, 524.
(56) Hawtin, R. W.; Rodger, P. M. *J. Mater. Chem.* **2006**, *16*, 1934.
(57) Moon, C.; Hawtin, R. W.; Rodger, P. M. *Faraday Discuss.* **2007**, *136*, 367.
(58) Gómez Gualdrón, D. A.; Balbuena, P. B. *J. Phys. Chem. C* **2007**, *111*, 15554.
(59) Bagherzadeh, S. A.; Alavi, S.; Ripmeester, J. A.; Englezos, P. *Phys. Chem. Chem. Phys.* **2015**, *17*, 9984.
(60) Hess, B.; Kutzner, C.; van der Spoel, D.; Lindahl, E. *J. Chem. Theory Comput.* **2008**, *4*, 435.

DOI: 10.1021/jacs.5b07417
J. Am. Chem. Soc. 2015, 137, 12079−12085

(61) Van der Spoel, D.; Lindahl, E.; Hess, B.; Groenhof, G.; Mark, A. E.; Berendsen, H. J. C. *J. Comput. Chem.* **2005**, *26*, 1701.
(62) Abascal, J. L. F.; Vega, C. *J. Chem. Phys.* **2005**, *123*, 234505.
(63) Jorgensen, W. L.; Madura, J. D.; Swenson, C. J. *J. Am. Chem. Soc.* **1984**, *106*, 6638.
(64) Schicks, J. M.; Ripmeester, J. A. *Angew. Chem., Int. Ed.* **2004**, *43*, 3310.
(65) Matsumoto, M.; Tanaka, H. *J. Phys. Chem. B* **2011**, *115*, 8257.
(66) Kumar, S.; Rosenberg, J. M.; Bouzida, D.; Swendsen, R. H.; Kollman, P. A. *J. Comput. Chem.* **1992**, *13*, 1011.
(67) Hub, J. S.; de Groot, B. L.; van der Spoel, D. *J. Chem. Theory Comput.* **2010**, *6*, 3713.
(68) Cornell, W. D.; Cieplak, P.; Bayly, C. I.; Gould, I. R.; Merz, K. M.; Ferguson, D. M.; Spellmeyer, D. C.; Fox, T.; Caldwell, J. W.; Kollman, P. A. *J. Am. Chem. Soc.* **1995**, *117*, 5179.
(69) Jorgensen, W. L.; Tirado-Rives, J. *J. Am. Chem. Soc.* **1988**, *110*, 1657.
(70) Frisch, M. J.; Trucks, G. W.; Schlegel, H. B.; Scuseria, G. E.; Robb, M. A.; Cheeseman, J. R.; Scalmani, G.; Barone, V.; Mennucci, B.; Petersson, G. A.; Nakatsuji, H.; Caricato, M.; Li, X.; Hratchian, H. P.; Izmaylov, A. F.; Bloino, J.; Zheng, G.; Sonnenberg, J. L.; Hada, M.; Ehara, M.; Toyota, K.; Fukuda, R.; Hasegawa, J.; Ishida, M.; Nakajima, T.; Honda, Y.; Kitao, O.; Nakai, H.; Vreven, T.; Montgomery, J. A., Jr.; Peralta, J. E.; Ogliaro, F.; Bearpark, M. J.; Heyd, J.; Brothers, E. N.; Kudin, K. N.; Staroverov, V. N.; Kobayashi, R.; Normand, J.; Raghavachari, K.; Rendell, A. P.; Burant, J. C.; Iyengar, S. S.; Tomasi, J.; Cossi, M.; Rega, N.; Millam, N. J.; Klene, M.; Knox, J. E.; Cross, J. B.; Bakken, V.; Adamo, C.; Jaramillo, J.; Gomperts, R.; Stratmann, R. E.; Yazyev, O.; Austin, A. J.; Cammi, R.; Pomelli, C.; Ochterski, J. W.; Martin, R. L.; Morokuma, K.; Zakrzewski, V. G.; Voth, G. A.; Salvador, P.; Dannenberg, J. J.; Dapprich, S.; Daniels, A. D.; Farkas, Ö.; Foresman, J. B.; Ortiz, J. V.; Cioslowski, J.; Fox, D. J. *Gaussian 09*; Gaussian, Inc.: Wallingford, CT, 2009.
(71) Singh, U. C.; Kollman, P. A. *J. Comput. Chem.* **1984**, *5*, 129.
(72) Besler, B. H.; Merz, K. M.; Kollman, P. A. *J. Comput. Chem.* **1990**, *11*, 431.
(73) Pohorille, A.; Pratt, L. R. *J. Am. Chem. Soc.* **1990**, *112*, 5066.
(74) Chandler, D. *Nature* **2005**, *437*, 640.
(75) Yu, H. A.; Karplus, M. *J. Chem. Phys.* **1988**, *89*, 2366.
(76) Yagasaki, T.; Iwahashi, K.; Saito, S.; Ohmine, I. *J. Chem. Phys.* **2005**, *122*, 144504.
(77) Yagasaki, T.; Saito, S.; Ohmine, I. *J. Phys. Chem. A* **2010**, *114*, 12573.
(78) Bennett, C. H. *J. Comput. Phys.* **1976**, *22*, 245.
(79) Beutler, T. C.; Mark, A. E.; van Schaik, R. C.; Gerber, P. R.; van Gunsteren, W. F. *Chem. Phys. Lett.* **1994**, *222*, 529.
(80) Wallqvist, A. *J. Chem. Phys.* **1992**, *96*, 5377.
(81) Koga, K.; Tanaka, H.; Nakanishi, K. *J. Chem. Phys.* **1994**, *101*, 3127.
(82) Shin, K.; Kumar, R.; Udachin, K. A.; Alavi, S.; Ripmeester, J. A. *Proc. Natl. Acad. Sci. U. S. A.* **2012**, *109*, 14785.
(83) Shin, K.; Udachin, K. A.; Moudrakovski, I. L.; Leek, D. M.; Alavi, S.; Ratcliffe, C. I.; Ripmeester, J. A. *Proc. Natl. Acad. Sci. U. S. A.* **2013**, *110*, 8437.
(84) Alavi, S.; Shin, K.; Ripmeester, J. A. *J. Chem. Eng. Data* **2015**, *60*, 389.
(85) Chapoy, A.; Anderson, R.; Tohidi, B. *J. Am. Chem. Soc.* **2007**, *129*, 746.
(86) Wataru, S.; Takao, E.; Hiroyuki, O.; Yasushi, K.; Satoshi, T.; Tsutomu, U.; Jiro, N.; Hideo, N. *Jpn. J. Appl. Phys.* **2003**, *42*, L129.
(87) Sakamoto, H.; Sato, K.; Shiraiwa, K.; Takeya, S.; Nakajima, M.; Ohmura, R. *RSC Adv.* **2011**, *1*, 315.

DOI: 10.1021/jacs.5b07417
J. Am. Chem. Soc. 2015, 137, 12079−12085